Sensors & Actuators: B. Chemical 314 (2020) 128074

Contents lists available at ScienceDirect

Sensors and Actuators B: Chemical

journal homepage: www.elsevier.com/locate/snb

Pressure self-compensation for humidity sensing using graphene-oxide-modified dual-frequency CMUT

Xiaoli Zhang[a], Xingguo Zhang[a], Xiaochen Lai[a], Ridong Wang[a], Haixia Yu[b], Dachao Li[a,*]

[a] State Key Laboratory of Precision Measuring Technology and Instruments, Tianjin University, Tianjin, China
[b] Tianjin Key Laboratory of Biomedical Detecting Techniques and Instruments, Tianjin University, Tianjin, China

ARTICLE INFO

Keywords:
CMUT
Dual-frequency
Pressure self-compensation
Humidity sensing
Graphene oxide

ABSTRACT

Capacitive micro-machined ultrasonic transducer (CMUT) has emerged as a promising candidate for gravimetric humidity sensing applications for its unique advantages. However, the measurement accuracy is badly influenced by the ambient pressure especially in the occasions of large pressure change such as meteorological observation. Therefore, a novel dual-frequency CMUT was proposed for pressure self-compensation during humidity measurement for the first time. The pressure self-compensation was carried out by obtaining the humidity measurement curves under different pressures. The CMUT sensor was designed with two resonant frequencies of 180 kHz and 1.8 MHz. Firstly, the pressure was detected by measuring the frequency shift around 180 kHz and this frequency was almost not affected by the humidity conditions. Then the relative humidity (RH) could be acquired through the resonant frequency shift around 1.8 MHz in RH of 30 %–90 % at this pressure. The cells of 1.8 MHz were functionalized by graphene oxide (GO) to improve the sensitivity of humidity sensing. The results demonstrated that the dual-frequency sensor showed high sensitivity for pressure detection and exhibited good sensitivity for RH sensing under different pressures, for example the sensitivity at 1 atm is 1.96 kHz/%RH for RH of 60 %–90 % and 663 Hz/%RH for RH of 30 %–60 %. Decent repeatability was also achieved by the CMUT sensor. What's more, this dual-frequency sensor can be used in the cases where simultaneous detection of pressure and humidity is necessary. Compared with detection of pressure and humidity simultaneously by two sensors, this CMUT sensor owns many advantages such as small volume, low cost, high consistency as well as easy operation.

1. Introduction

Humidity is a crucial environmental parameter in many fields such as medicine, agriculture, and industry [1–4]. The types of humidity sensors consist of capacitive [5], resistive [6,7], optical [8], piezoresistive [9] and gravimetric [10]. Among these sensors, the gravimetric ones offer advantages such as high sensitivity and fast response [11]. The mechanism is that the resonant frequency of the sensor will shift when an additional mass is deposited on the sensing film [12]. Quartz crystal microbalance (QCM) [13,14], surface acoustic wave (SAW) sensors [15,16], film bulk acoustic resonators (FBARs) [17], and micro-cantilevers [18] have been widely used as gravimetric humidity sensors. In recent research, capacitive micro-machined ultrasonic transducer (CMUT) [19] has emerged as a promising gravimetric humidity sensor for its unique advantages. First, the resonant thin membrane is backed by a vacuum cavity, which reduces the energy loss to improve the quality factor and facilitates to functionalize the sensitive layers on one side of the sensor [20]. Second, the sensor is made of many resonators connected in parallel. This multi-resonator structure has three main advantages: low thermal noise to improve the quality of detecting the small signal, a wide range of electrical impedance to match to electronics and an enhanced reliability compared to a single-resonator system [21].

Several research groups have used CMUTs as sensitive humidity sensors. In 2012, Lee et al. presented a mesoporous silica thin film on a highly sensitive miniaturized CMUT for relative humidity (RH) detection and reported a sensitive detection of 2 kHz/%RH to water vapor [22]. In 2014, Lee et al. applied CMUT to detect water vapors using mesoporous silica and guanidine polymer as sensing materials, respectively, the corresponding sensitivities of 1.172 kHz/%RH and 2.6 kHz/%RH were reported in an RH range of 0 %–20 % [23]. In 2019, Zheng et al. presented a CMUT-based humidity sensor functionalized with graphene oxide (GO), which showed an excellent sensitivity of up to 11.5 kHz/%RH between an RH level of 22.5 %–93.6 % [10]. Later,

* Corresponding author.
E-mail address: dchli@tju.edu.cn (D. Li).

https://doi.org/10.1016/j.snb.2020.128074
Received 14 January 2020; Received in revised form 29 March 2020; Accepted 31 March 2020
Available online 08 April 2020
0925-4005/

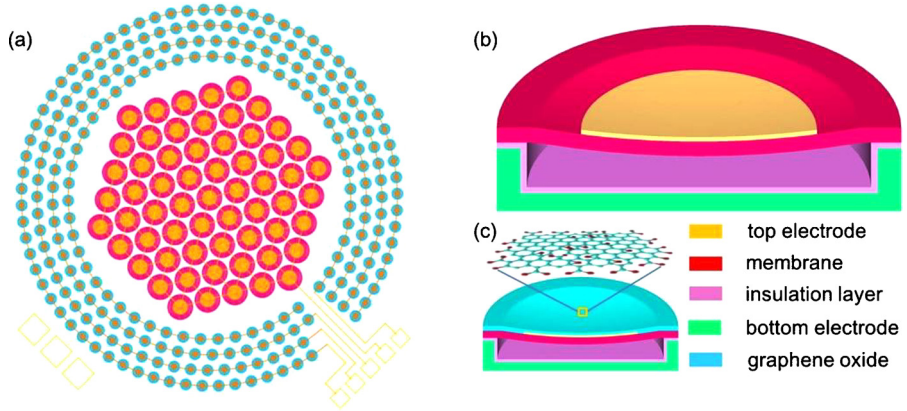

Fig. 1. (a) structure diagram of the dual-frequency CMUT; (b) the profile of big CMUT cell in the middle; (c) the profile of small CMUT cell in the periphery and the functionalized GO film.

Zheng et al. improved the performance of CMUT with nitride-to-oxide wafer bonding technology and achieved 15.3 kHz/%RH [19]. Although CMUT owns many advantages in humidity sensing by monitoring the frequency shifts of the sensor, the ambient pressure can also change the resonant frequency of the sensor over time due to the membrane structure of CMUT [24]. Hence it is unable to make continuous humidity measurements with this sensor, which is a key problem that needs to be solved for CMUT humidity sensing. Therefore, the pressure compensation during CMUT humidity sensing to improve the stability of humidity measurement is of great significance [25].

In the last few years, CMUT sensors have also been demonstrated as competitive MEMS resonant pressure sensors which measures external pressure by detecting a change in the resonant frequency. Min-Chieh et al. [26] operated the CMUT in permanent contact mode and demonstrated its functionality under 1–20 atm ambient pressure. Nikhil et al. [27] proposed CMUT with vented cavities for pressure detection which prevented mechanical failure. Li et al. [28] also used a CMUT for an ultralow pressure measurement. The authors showed that the resonant frequency of the CMUT varied linearly with the applied pressure, and the membranes of biased CMUTs could produce a larger resonance frequency shift than those without a DC bias. But the authors did not conduct experiments to demonstrate these results. And, the two types of pressure detection mechanism for CMUT have been thoroughly investigated through theory analysis and experiments in our previous research [29]. However, CMUT was only used for pressure detection in these researches.

Excitingly, the CMUT sensor can be a broadband device by designing different membrane dimensions on the same substrate using the same fabrication process. By innovatively making use of the unique broadband characteristic of CMUT, we first proposed and designed a dual-frequency CMUT sensor to make in-situ pressure compensation during the humidity measurement in this paper. What's more, this proposed sensor could also be used to detect pressure and humidity simultaneously in some cases, for instance, meteorological observation, environment monitoring in space suits, conditions controlling in laboratory glove boxes and heat-humidity sterilizers [30–32].

To design such a sensor, three aspects needed to be considered: the pressure range, the sensitive layer for humidity sensing and the fabrication method. Firstly, considering the applications of meteorological observation, environment monitoring in space suits, conditions controlling in laboratory glove boxes and heat-humidity sterilizers, the pressure range from negative pressure to one atm was to be measured. Secondly, the GO, which had a large surface volume ratio and hydrophilic functional groups, was reported with the best humidity sensitivity for humidity measurement [19]. And GO also had good electrical insulation properties and could be directly deposited on the membrane surface of CMUT [33]. Hence GO was adopted as the sensitive layer in this paper. Thirdly, the wafer bonding method, with which the silicon-on-insulator (SOI) wafer was directly bonded with the low-resistivity silicon substrate, was adopted in this paper. This method was easy to implement the fabrication of the dual-frequency CMUT sensor [34]. The device layer of SOI wafer was employed as the membranes of CMUT cells, thus the membranes had good thickness uniformity and were favorable for good sensor performance. Closed and flat membrane surface generated by this method was easy to be functionalized, which was also a big advantage of CMUT over traditional humidity sensors [35].

In this paper, a dual-frequency CMUT sensor was designed, simulated and fabricated to make in-situ pressure compensation for RH measurement. The sensor resonant frequencies and uniformities were characterized by a vector network analyzer after fabrication. Then only the CMUT cells of 1.8 MHz were functionalized with GO sensitive layer for humidity sensing. At last, a detection system was set up for pressure and humidity measurement using the dual-frequency CMUT sensor. The pressure was directly detected by measuring the frequency shift of the 180 kHz. And the humidity sensing performance was investigated through the frequency shift of the 1.8 MHz under different pressures. The sensitivity and repeatability of the sensor for RH sensing were also characterized.

2. The dual-frequency CMUT sensor

2.1. Design and operational principle

In this paper, a dual-frequency CMUT sensor is designed to detect pressure and RH simultaneously for pressure self-compensation during humidity sensing. As shown in Fig. 1(a), the sensor is consisted of the inside big cells and the outside small cells which are used to measure pressure and RH, respectively. The big cells are connected to each other and distribute in the middle to avoid rupture during the splinter process after fabrication. While the small cells are interconnected in each circle and distribute in the periphery. The different circles can be linked together during the measurements. In addition, the big cells are arranged into a hexagon instead of circular rings to facilitate the GO modification of the small cells for that GO is not easily modified to the middle area because of the space around the hexagon.

The big and small cells in the CMUT array are all composed of drum-like resonator structures. And, as shown in Fig. 1(b) and (c), each resonator consists of a metalized (work as top electrode) moving membrane and a rigid doped substrate (work as bottom electrode) separated by an insulation layer and a vacuum cavity [36]. When an AC voltage is added upon the DC biased electrodes, the membrane vibrates. Two important design parameters for CMUT are the resonant frequency and the pull-in voltage.

The pull-in voltage is defined as the DC voltage beyond which the membrane will be in contact with the insulation layer suddenly. The pull-in voltage can be expressed as:

$$V_{pull-in} = \sqrt{\frac{8k_s {d_{eff}}^3}{27A\varepsilon_0}} \tag{1}$$

where $A = \pi a^2$ is the membrane area, ε_0 is the permittivity of vacuum, k_s is the spring constant of the moving membrane, d_{eff} is the effective cavity depth [37]. The pull-in voltage can be designed by adjusting the radius and the effective cavity depth. And the two kinds of cells have different pull-in voltages, which can be expressed as $V_{pull-in}|_{\text{pressure}}$ and $V_{pull-in}|_{\text{humidity}}$, respectively. The DC voltage used for all the cells will be set as a specified value that is below both $V_{pull-in}|_{\text{pressure}}$ and $V_{pull-in}|_{\text{humidity}}$.

The resonant frequency of a circular CMUT cell can be expressed as [38]:

$$f_0 = 0.47\frac{t}{a^2}\sqrt{\frac{E}{\rho(1-\nu^2)}} = \frac{0.83}{a}\sqrt{\frac{Et^3}{m(1-\nu^2)}} \tag{2}$$

where t, a, E, ρ and ν are the thickness, radius, Young's modulus, density, and Poisson's ratio of the membrane, respectively. And m is the mass of the membrane which can be calculated by $m = \pi a^2 t\rho$. When the ambient water molecule with mass of δm was adsorbed by the GO film distributed on the membranes of the small cells, the mass of the membrane was increased. Then f_0 decreases based on Eq. (2). That is, f_0, which is related to the mass of the membrane, can be used for RH sensing.

If the loaded mass is small compared with the mass of the membrane, the mass sensitivity is obtained as [39]:

$$S = \frac{\delta f_0}{\delta m} = -\frac{1}{2}\frac{f_0}{m} \propto \frac{1}{a^4} \tag{3}$$

Eq. (3) indicates that S is inversely proportional to m, and directly proportionally to f_0. And based on Eq. (2), f_0 is directly proportional to the thickness t and inversely proportional to the square of the radius a. So $S \propto 1/a^4$. Therefore the mass sensitivity can be improved by decreasing the radius a. Hence, the CMUT cells with small radius and sensitive layer modification were designed for humidity sensing.

The principle of pressure detection is that ambient pressure can shift the resonant frequency of CMUT by changing the stiffness coefficient of the CMUT membranes. In general, CMUT cell is a resonant structure similar to a mass loaded spring. Its resonant frequency can be approximately expressed as:

$$f_0 = \sqrt{\frac{k_s}{m}} \tag{4}$$

where k_s is the equivalent stiffness coefficient and m is the mass of the vibrating membrane. According to our previous study [29], the large deflection theory is adopted in this paper because of the wide pressure range to be measured. In this theory, k_s increases as the ambient pressure increases, and then the resonant frequency increases according to Eq. (4).

2.2. Determination of the structure parameters

To optimize the structural parameters of CMUT, a finite element model (FEM) was created in COMSOL Multiphysics (COMSOL, Inc., Burlington, MA, USA) to simulate the performance of the CMUT cells. All the mechanical and electrical properties (density of ρ, Young's modulus of E, Poisson's ratio of ν, and relative permittivity of ε_γ) of the materials from previous study [29] were used. Fig. 2 shows the design of two-dimensional (2D) axisymmetric FEM. In this paper, wafer bonding technology was selected to fabricate the dual-frequency sensor. The thickness of the membrane, which was dependent on the device layer of SOI, was set to 10 μm for all the cells. And a 2 μm-thick insulation layer was used to isolate the conductive silicon substrate from the top electrode.

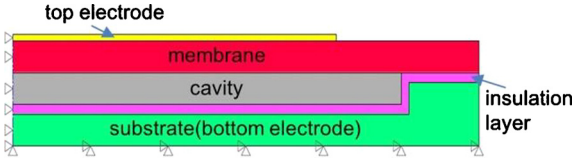

Fig. 2. The 2-D finite element model of CMUT in COMSOL.

In this paper, the pressure range of 20 kPa to 1 atm was detected. As the large deflection theory was adopted, a large $V_{pull-in}|_{\text{pressure}}$ was to be designed in this theory. According to Eq. (1), small radius and large cavity depth were preferred to increase the pull-in voltage. However, based on the mass loading effect of CMUT sensor for RH in Section 2.1, large radius could reduce the influence of humidity on the pressure detection. Then several groups of parameters were selected for simulation. The DC voltage of 120 V was used for all the simulations. As shown in Fig. 3(a), when the cavity depth was fixed and the radius increased from 380 μm to 480 μm, the sensitivity increased from 135 Hz/kPa to 406 Hz/kPa while the R-square increased from 0.958 to 0.992. It could be seen that the larger radius had the larger pressure detection sensitivity. In addition, the cells with larger radius were less sensitive to RH variations to ensure the pressure self-compensation for RH measurement. Hence the large radius was preferred. But the membrane with radius higher than 480 μm was likely to pull in at one atmosphere. Therefore, the radius of 480 μm was fixed and the cavity depth was increased from 8 μm to 11 μm for simulation, as shown in Fig. 3(b), the sensitivity increased from 371 Hz/kPa to 410 Hz/kPa while the R-square decreased from 0.9953 to 0.9912. Hence any cavity depth value of 9 μm, 10 μm and 11 μm could be selected for that the sensitivity and the linearity changed slowly as the cavity depth was larger than 9 μm. Finally the radius of 480 μm and cavity depth of 10 μm were chosen for fabrication. Then the detection sensitivity and linearity at different voltages of 30 V, 60 V, 90 V, 120 V, and 150 V were simulated to optimize the driven DC voltage, which were listed in Table 1. As the DC voltage became larger, the sensitivity decreased from 411.75 Hz/kPa to 402.13 Hz/kPa while the linearity increased from 0.9907 to 0.9921. Hence any voltage between 30 V–150 V could be used to realize the pressure detection.

For RH sensing, the resonant frequency decreased as the load mass of adsorbed water molecules increased. For it was difficult to simulate the actual adsorption amount of water molecules by GO film in the FEM, the structural parameters of CMUT cells for humidity sensing were determined through theoretical analysis. According to Eq. (3), the mass sensitivity of humidity sensing could be improved by decreasing the radius to increase the resonant frequency and reduce the mass. What's more, the DC voltage closer to $V_{pull-in}|_{\text{humidity}}$ could lead to higher mass sensitivity [40], thus $V_{pull-in}|_{\text{humidity}}$ should be designed in acceptable range for that the DC voltage could not be very high in practical applications. According to Eq. (1), the pull-in voltage could be reduced by increasing the radius and decreasing the effective cavity depth. It could be observed that the design criterion of the membrane radius was contradictory for improving the mass sensitivity and reducing the pull-in voltage. Therefore, as the radius was reduced to improve the mass sensitivity, the cavity depth needed to be smaller to reduce the pull-in voltage. Considering the difficulty of actual processing technology, the cavity depth was selected as 0.6 μm. Several groups of parameters were selected for simulation of the resonant frequencies and pull-in voltages in the FEM model, as shown in Table 2. The resonant frequency as well as the $V_{pull-in}|_{\text{humidity}}$ increased as the radius was decreased. Finally the cells of 1.8 MHz with radius of 130 μm and cavity depth of 0.6 μm was chosen for humidity detection. The actual performance would be investigated by the experiments. According to the analysis above, the critical structure parameters were

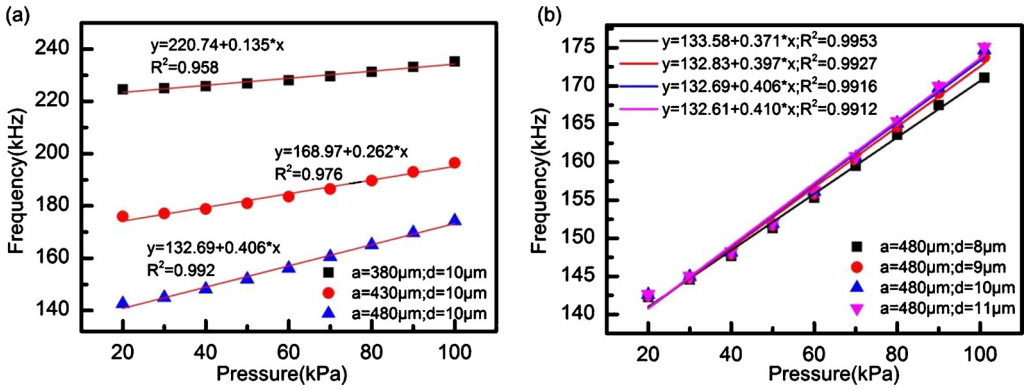

Fig. 3. (a) the resonant frequency curves of big CMUT cells with radius of 380 μm, 430 μm, 480 μm and cavity depth of 10μm at 120 V under pressures of 20-101 kPa; (b) the resonant frequency curves of big CMUT cells with radius of 480 μm and cavity depth of 8 μm, 9 μm, 10 μm, 11 μm at 120 V under pressures of 20-101 kPa.

Table 1
The sensitivity and linearity of big cells with radius of 480 μm and cavity depth of 10 μm for pressure detection of 20kPa-1 atm at different voltages.

DC voltage(V)	Sensitivity(Hz/kPa)	R-Square
30	411.75	0.9907
60	410.58	0.9909
90	408.67	0.9912
120	405.88	0.9916
150	402.13	0.9921

Table 2
The simulation results of resonant frequencies and pull-in voltages for different dimensions of small cells.

	radius = 100 μm cavity depth = 0.6 μm	radius = 130 μm cavity depth = 0.6 μm	radius = 180 μm cavity depth = 0.6 μm
$V_{pull-in}\|_{humidity}$	581 V	341 V	160 V
Resonant frequency	2.93 MHz	1.76 MHz	863.25 kHz

Table 3
The structure parameters of big and small cells in the dual-frequency CMUT.

Layer	Dimensions of big cells		Dimensions of small cells	
	radius/μm	thickness/μm	radius/μm	thickness/μm
Top electrode	350	0.2	90	0.2
Membrane	480	10	130	10
Cavity	480	10	130	0.6
Insulation layer	480	2	130	2

presented in Table 3.

In summary, firstly, as the detection mechanism of CMUT sensor for pressure and RH were different, so two different frequencies of 180 kHz and 1.8 MHz were designed to improve the detection sensitivities for both parameters. After simulation, calculation and optimization, the cells with radius of 130 μm and cavity depth of 0.6 μm, which had the resonant frequency of 1.8 MHz, were chosen for RH measurement. The cells with radius of 480 μm and cavity depth of 10 μm, which had the resonant frequency of 180 kHz, were chosen for pressure detection.

Secondly, based on the mass loading effect of CMUT sensor for RH, the 180 kHz cells with larger radius were less sensitive to RH variations. It meant that the structure at 180 kHz not only had better sensitivity for pressure detection, but also largely reduced the influence of humidity conditions on pressure detection. Hence the ambient pressure could be detected by the big cells directly which ensured the pressure self-compensation for RH measurement.

3. Fabrication of the dual-frequency CMUT

3.1. Sensor fabrication

The wafer bonding process was adopted for the fabrication of the dual-frequency CMUT sensor, which would increase the yield, uniformity, and process control [41]. Fig. 4 showed the fabrication procedures of the dual-frequency CMUT. It began with the thermal oxidation of a low resistivity silicon wafer to a pre-determined thickness. The cavity shapes of the big cells were then patterned on the oxide layer using photolithography method, and the cavity was formed by dry etch method. After that, another layer of silicon dioxide was thermally grown. Similarly, the small cells could be obtained by repeating the above two steps. The silicon dioxide layer in Fig. 4d was used as an isolation layer for the dual-frequency CMUT. After that, the wafer with cavities was then bonded with the SOI wafer under vacuum. The handle of the SOI wafer and the buried oxide layer were removed to release the active silicon layer which constituted the membranes of the CMUT sensor. Then a film of Au was sputtered on the membranes of the CMUT cells, the Au electrodes of big cells were connected in parallel and drawn out as the top electrode 1 (E1). Likewise, the top electrode 2 (E2) was drawn out for connections to the small cells. At last, openings were defined and etched to gain access to the low resistivity silicon layer, and a film of Au was sputtered and patterned to establish the connections to the common bottom electrode (G). The bottom electrode was used for both the large and small cells.

3.2. Sensor characterization

The static and resonant performances of the CMUT sensor were explored before GO functionalization. CMUT cell had a vacuum cavity and would produce static displacement when atmospheric pressure was applied to the membrane. Note that the static displacement of the CMUT cell was actually the deformation of the CMUT membrane. Fig. 5(a) and (b) showed the static simulation results of the big and small cell, respectively. The substrate was omitted in these simulation processes for simplifying the FEM analysis, which had no effect on the results because the substrate had no degrees of freedom. It could be seen that the center of the clamped circular membrane had the largest displacement, which were 6.49 μm and 0.04 μm for the big and small membranes, respectively.

The white light interferometer was used to observe the actual static displacements of the fabricated big and small membrane, as shown in Fig. 5(c) and (d). According to Fig. 5(c), the big membrane deformed to the bottom obviously with the largest deformation at the center point. And the displacement of the central point of the membrane was 6.3978 μm in relation to the non-membrane position. Similarly, the small membrane had a measured deformation of 28.28 nm according to

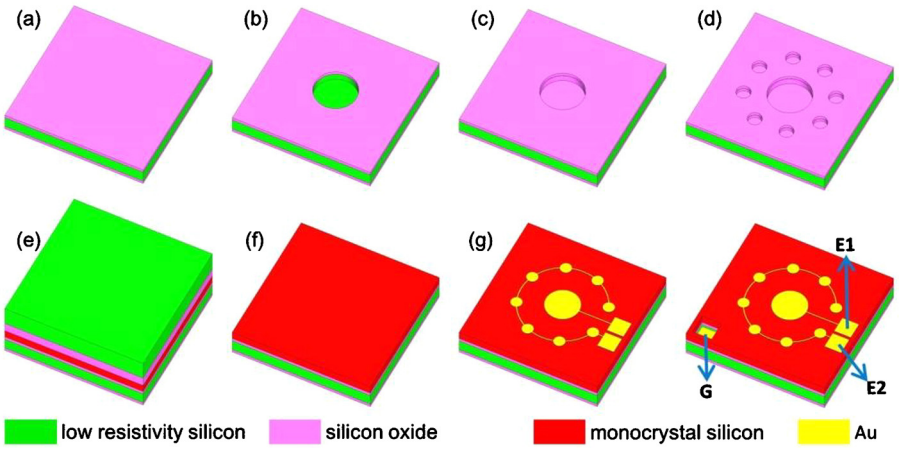

Fig. 4. Fabrication process of the dual-frequency CMUT: (a) first thermal oxidation step; (b) cavity definition of big cells with photolithography and etch; (c) thermally grown silicon oxide; (d) cavity definition of small cells and thermal oxidation; (e) silicon direct bonding of the patterned prime wafer to the SOI wafer; (f) removal of the handle and the buried oxide layer of the SOI wafer to release the membranes; (g) top electrode deposition, and patterning; (h) bottom electrode definition.

Fig. 5(d). Though the measured static displacements had some deviations from the simulated results, the simulation could predict well when comparing the simulation results with the experimental results. The deviations mainly came from the material and structural parameters differences between theoretical model and the fabricated sensor. The deviation of the small membrane was more obvious due to that the differences between the simulation and actual parameters were more influential for the small membrane. In addition, the roughness of the small membrane surface led to the small burrs on the measurement curve. The burrs were not observed in Fig. 5(c) due to that the roughness was negligible compared with the displacement of the big membrane.

Then the impedance analyzer was employed to excite the CMUT and test the generated electrical characteristics of the CMUT to analyze the first-order resonant frequency and the consistency between the cells. Fig. 6 showed the electrical characteristic curves of the big and small cells under DC voltages of 30 − 180 V which were lower than the pull-in voltages of both cells. Fig. 6(a) and (c) were the impedance and phase

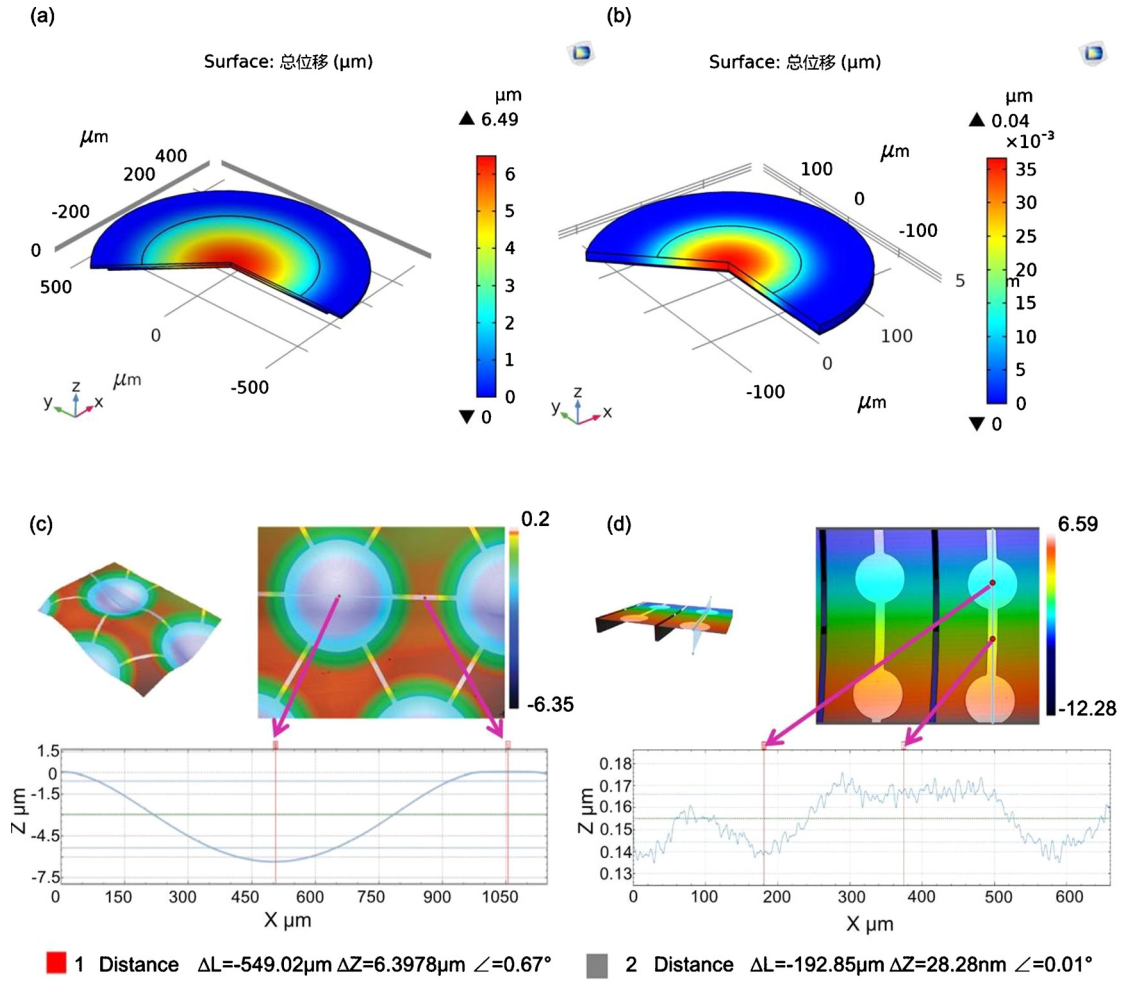

Fig. 5. (a) the simulated displacement of big membrane; (b) the simulated displacement of small membrane; (c) the measured displacement of big membrane; (d) the measured displacement of small membrane.

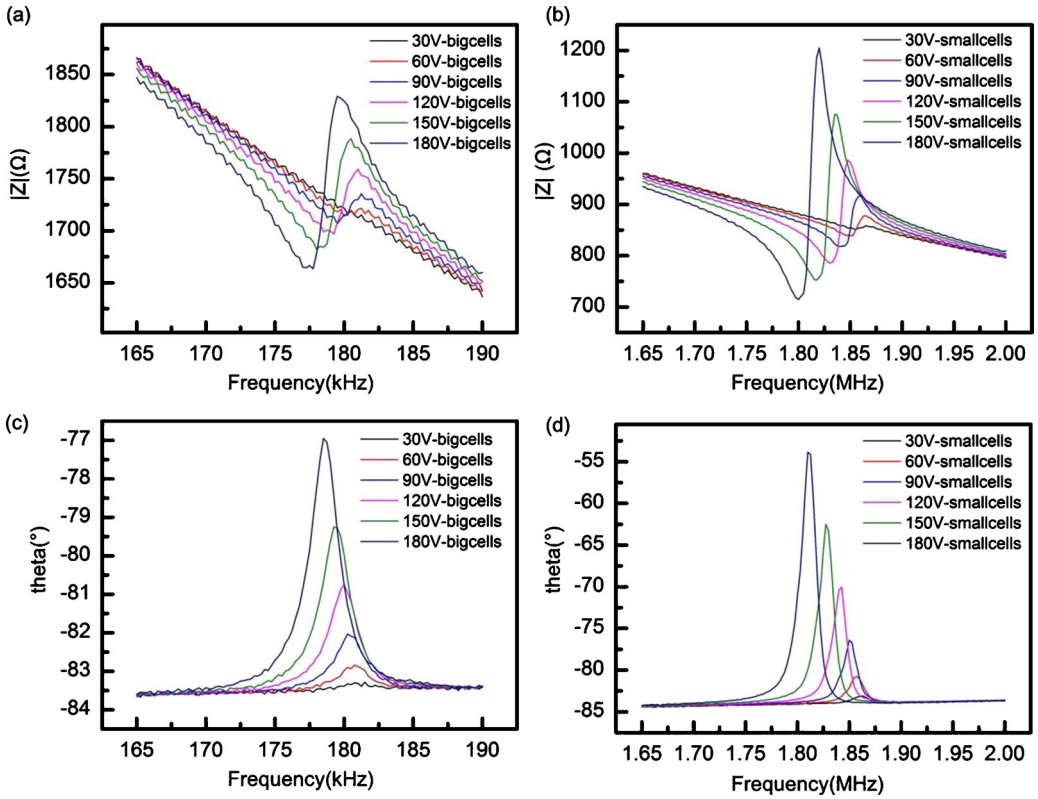

Fig. 6. (a) the electrical impedance curves of big cells; (b) the electrical impedance curves of small cells; (c) the phase curves of big cells; (d) the phase curves of small cells.

curves of the big cells. Series and parallel resonant frequencies were obtained from the impedance curves with the minimum and maximum impedance at the abrupt variation of impedance. Because of the sparse sampling, the impedance curves had a little fluctuation but it didn't affect the measurement of the resonant frequency. The resonant frequency decreased as the DC voltage became larger because of the spring softening effect. This effect could be explained as follows: An electrostatic force was generated when a DC voltage was applied between the top and bottom electrodes. Due to the electrostatic force, the top electrode was pulled towards the bottom electrode. The decreased gap between the top and bottom electrodes further increased the electrostatic force, thus the displacement of the membrane was further increased. So according to $k_s = F/x$, the spring constant was decreased, and f_0 was correspondingly decreased based on Eq. (4). In addition, the spring softening effect was more obvious as the DC voltage was closer to the pull-in voltage. The amplitude of phase change reflected the vibration amplitude of the membrane. As shown in Fig. 6(c), the phase change increased with the increase of the DC voltage, which indicated that the larger DC voltage resulted in the larger vibration amplitude.

Fig. 6(b) and (d) were impedance and phase curves of the small cells. With the increase of DC voltage, the variations of impedance and phase were similar to that of the big cells. Compared with the big cells, the frequency shift of the small cells was more obvious with the increase of DC voltage. That was because the spring softening effect of the same DC voltage was more obvious for the small cells as the pull-in voltage of the small cells was small. From all the figures, it could be observed that the electric impedance curve was more stable and the resonant peak was more obvious by increasing the DC voltage. However, DC voltage should not be too large in practical applications; hence the voltage of 120 V was adopted for biasing the two kinds of cells.

3.3. Sensor modification

The most often used techniques for functionalization of the gravimetric sensors were electrochemical method and spin coating method. However, the electrochemical method and the spin coating method were suitable for modifying the whole surface of the sensor [42]. But only small cells of the dual-frequency sensor needed to be functionalized here. Therefore, a very simple drop coating method was chosen. 100 μL 1 mg/mL GO water solution (Nanjing XFNANO Materials Tech Co., China) was sampled by the pipette chamber and dropped on the surface of small CMUT cells. Then the sensor was left at room temperature for one day, and the function layer was formed with the evaporation of solvent. A scanning electron microscope (SEM) image of the functionalized GO film on the small CMUT cells was shown in Fig. 7(a). It could be seen that the film generated on the surface of the small cells by drop coating had good uniformity. At DC voltage of 120 V, the electrical phase curves of CMUT before and after coating GO film were characterized, as shown in Fig. 7(b). The results showed that the resonant frequency of the small cells increased after modification. Eq. (2) indicated that the GO coating added the effective thickness of the CMUT membrane, thus increased the resonant frequency. And it also added an extra mass to the membrane, thus decreased the resonant frequency. Which effect dominated the frequency shift mainly depended on the dose of the GO. Here the thickness effect dominated and led to the increase of the resonant frequency. The phase values before and after functionalization were both negative according to Fig. 7(b). This was mainly due to the capacitive characteristics of the CMUT sensor. In addition, the phase change of the modified cells was smaller than that of the unmodified ones, indicating that the vibration amplitude of the modified cells was weakened. However, it had no effect on the measurement results for the resonant frequency could be clearly read out from the phase curve.

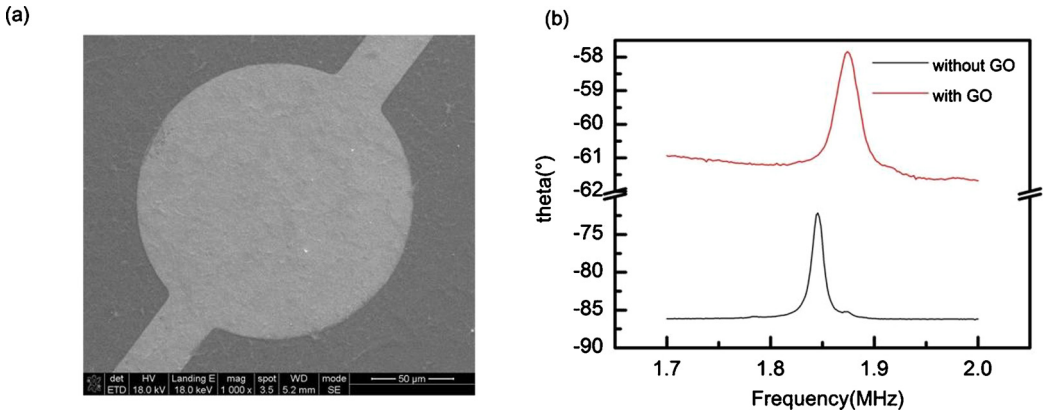

Fig. 7. (a) scanning electron microscope image of morphology of GO on the small CMUT membranes; (b) the phase curves of the small CMUT cells before and after coating GO film.

4. Experimental results and discussion

4.1. Experimental setup

The schematic diagram of the experimental system is shown in Fig. 8. The CMUT was placed in the chamber. Three wires, which went through the plug of the vent hole of the enclosure chamber, were used to connect the CMUT with the impedance analyzer fixuture. Three ends were connected to the top electrode (E1) of the big cells, the top electrode (E2) of the small cells and the common bottom electrode (G), respectively. The wires connecting E1 and G or E2 and G were successively placed in the high and low ports of the impedance analyzer fixture for monitoring of the impedence and phase curves of the big and small cells to obtain the resonant frequencies. DC power supplied the bias voltage for the CMUT through the fixture. The pump was used to extract or pump air into the chamber to adjust the pressure, which was displayed in real time by the pressure meter. The humidifier and drying agent were used to increase and decrease the RH in the chamber, and the real value was measured by the thermohygrograph. The resonant frequencies of the CMUT sensor were measured in a static mode in the enclosure chamber under different pressures and relative humidities. And these resonant frequencies could be obtained by the curves displayed on the impedance analyzer under a specific DC voltage. Note that all measurements were performed at room temperature.

4.2. The pressure detection characteristic of the sensor

Firstly, the electrodes of E1 and G were connected to the high and low ports of the fixture through wires. Then the pump was used to change the pressure in the enclosure chamber, and the pressure value in the chamber was read by the pressure meter. The impedance curves of the big cells of the CMUT at different DC voltages could be obtained at the given pressure. Correspondingly, the resonant frequency curves for pressure detection at different DC voltages could be acquired, as shown in Fig. 9(a).

As can be seen, the big cells of the CMUT exhibited good sensitivity and linearity in the pressure range of 20 − 101 kPa at different DC voltages. The pressure detection sensitivities were 437.62 Hz/kPa, 428.52 Hz/kPa, 408.49 Hz/kPa at 60 V, 120 V and 180 V, respectively. The sensitivity decreased a little from 60 to 180 V and the linearity increased a little with the increase of DC voltage, which agreed very well with the simulation results in Table 1. It can be also seen that at given pressure, the resonant frequency decreased a little as the DC voltage increased from 60 to 180 V because the pull-in voltage of big

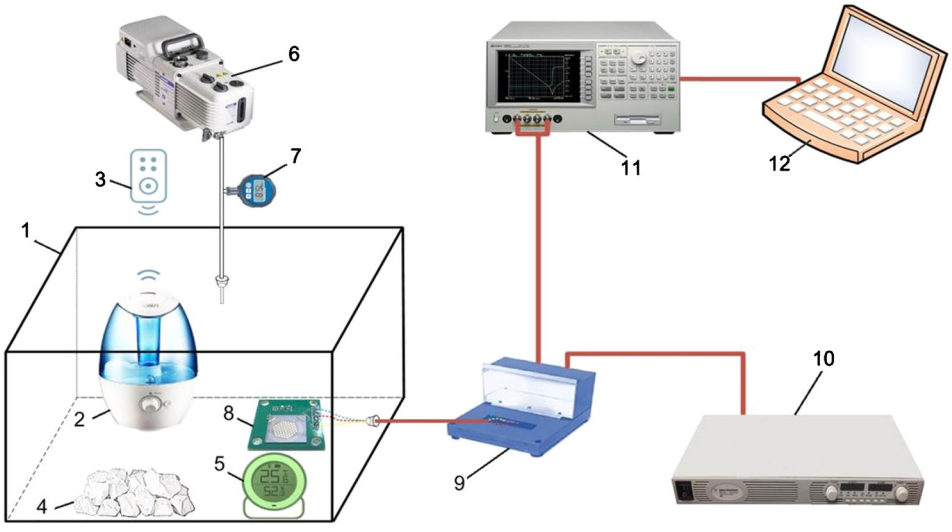

Fig. 8. The schematic diagram of the experiment setup for pressure detection and humidity sensing using the dual-frequency CMUT.

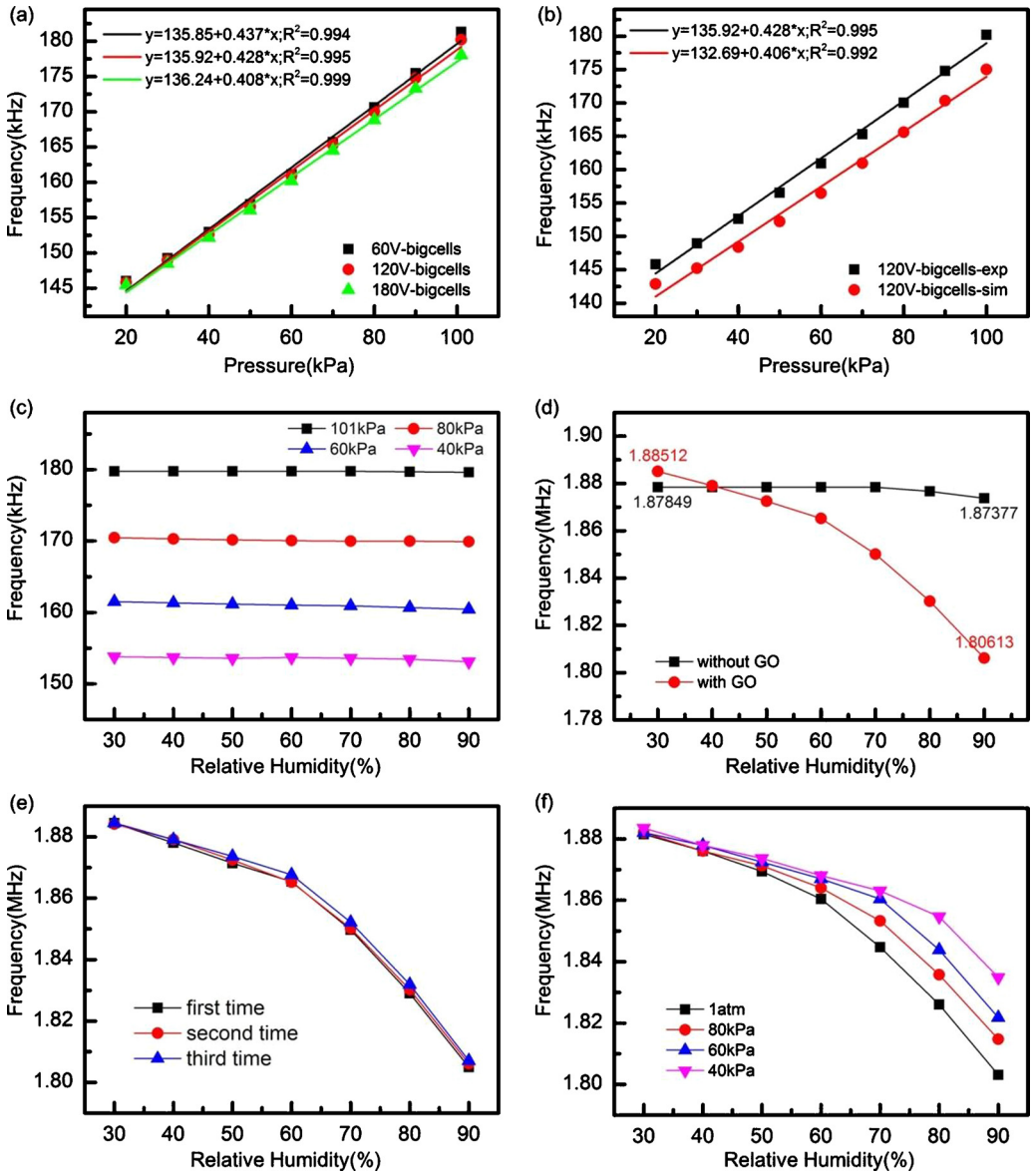

Fig. 9. (a) the resonant frequency curves of the big cells for pressure detection at different DC voltages; (b) comparison of the simulation and experiment results of the big cells at 120 V for pressure detection; (c) the resonant frequency curves of the big cells at RH of 30 %-90 % under different pressures; (d) the resonant frequency curves of the small cells at RH of 30 %-90 % coated with and without GO film; (e) the repeatability of the small cells coated with GO film for RH sensing of 30 %-90 %; (f) the resonant frequency curves of the small cells coated with GO at RH of 30 %-90 % under different pressures.

cells was high and the spring softening effect was not obvious. As shown in Fig. 9(b), though the resonant frequencies measured were a little higher than the simulation results, there still was a good consistence between the simulation and experimental results at 120 V. It was mainly because of the residual stress in the membranes introduced by the actual fabrication process. The slightly difference between the actual structural parameters and the designed parameters of the CMUT sensor also contributed to the difference between the simulation and experiment results.

The RH sensing performance of the big cells was characterized by measuring the resonant frequency as a function of RH level to investigate the influence of RH on the resonant frequency of the big cells. By linking the electrodes of E1 and G with the high and low ports of the impedance analyzer fxture, the resonant frequency curves of the biased big membranes could be acquired when the RH increased from 30 %–90 % under different pressures at 120 V, as shown in Fig. 9(c). It demonstrated that the RH had little influence on the frequency variation of the big cells at a specified pressure. The frequency shifts were 0.12 kHz, 0.54 kHz, 1.07 kHz, 0.69 kHz at pressures of 1 atm, 80 kPa, 60 kPa, and 40 kPa, respectively. It was analyzed that the lower resonant frequency of the big cells and the larger membrane radius led to worse mass sensitivity according to Eq. (3). What's more, the big cells were not coated with GO film. Therefore, the resonant frequencies of the big cells were less affected by the change of RH. Fig. 9(c) also showed that the resonant frequency changed a lot from 40 kPa to 101 kPa at a certain RH, which was consistent with the results in Fig. 9(a). As the ambient water molecules at low pressure was little and the humidity sensing was not so necessary at very low pressure, the pressure of 20 kPa was not measured. Based on Fig. 9(a) and (c), the resonant frequency shift of the big cells were mainly caused by the external pressure, so the pressure value could be directly measured according to the resonant frequency curves of the big cells for pressure detection in Fig. 9(a).

4.3. The humidity sensing characteristic of the sensor

In this paper, the RH measurements of the small cells coated with

Table 4
RH sensing performance of the small cells coated with GO.

Lable of sensors	RH	Humidity sensitivity (kHz/%RH)
with GO	30 %-60 % 60 %–90 %	0.663 1.96

and without GO film at 1 atm with DC voltage of 120 V were compared, as shown in Fig. 9(d). For uncoated CMUT cells, the frequency shift was ignorable ranging from 1.87849 MHz to 1.87377 MHz. The coated CMUT cells had a large frequency shift ranging from 1.88512 MHz to 1.80613 MHz. It was known that the RH sensing performance of the small cells was largely improved after coating GO film, which indicated that the sensitivity of the CMUT sensor depended on the sensitive layer that reacted with the water molecule. For coated CMUT cells, the humidity sensitivity were calculated within two ranges and summarized in Table 4. It is obvious that the humidity sensitivity was higher at high RH than that at low RH, for that more water molecules were adsorbed at high RH, hence the frequency shift was bigger and humidity sensitivity was higher. In addition, the linearity was good at low RH for that the water molecules were mainly concentrated on the surface of the GO film. When RH increased, water molecules gradually penetrated into the interlayer of GO film, resulting in a nonlinear increase in mass of the GO film.

The CMUT sensor for measuring RH level needed to show good repeatability. As shown in Fig. 9(e), the humidity measurements of the sensor were measured three times under 1 atm at 120 V to investigate the repeatability of the sensor. Repeatability error was calculated as the ratio of the maximum deviation of frequency shift to the full range of frequency shift. The maximum repeatability error of the CMUT sensor was 3.65 %, which indicated that the sensor had good repeatability for humidity sensing.

The resonant frequency curves to RH at different pressures were measured for the coated small cells, as shown in Fig. 9(f). When the RH was below 50 %, the frequency curves almost coincided under different pressures. However, the frequency shifts changed greatly under different pressures as the RH was higher than 50 %. This was because the water content was different under different pressures at the same RH, for example, the water content was higher at 1 atm than that at 60 kPa. So when the RH value was the same at low and high pressures, the water content at low pressure was less and the adsorption of water molecules was less, leading to a smaller frequency shift. Therefore, by using the dual-frequency CMUT sensor proposed in this paper, the RH value could be obtained according to the RH sensing curves under different pressures after the pressure was measured by the big cells of CMUT. Hence, the dual-frequency CMUT sensor proposed in this paper made up for the defect of existing humidity sensors which didn't correct the effect of pressure variation on their performances, and also realized simultaneous detection of pressure and humidity.

According to Eq. (3), the CMUT membranes can be designed small and thin to be more sensitive to the adsorption mass and then the detection sensitivity is increased. However, due to the limitation of materials in the laboratory, the humidity sensor designed in this paper has a relatively large diameter and a thick membrane, so the humidity detection sensitivity can be improved further by optimizing the structural parameters and the fabrication process which can also reduce the operating DC voltage. What's more, the detection circuit of the resonant frequency will be researched to realize the miniaturization of the detection system in the future.

5. Conclusion

In this paper, a novel dual-frequency CMUT was first proposed for pressure self-compensation during the humidity sensing process by taking advantage of the unique broadband characteristics of CMUT. The dual-frequency design not only improved the detection sensitivities for both pressure and RH, but also realized the pressure correction for the RH sensing. The CMUT array was designed, simulated, fabricated and the small cells of 1.8 MHz were functionalized by GO film to enhance the binding force with water molecules. The static and resonant performances of the CMUT sensor were characterized by white light interferometer and impedance analyzer, which showed good consistence with the finite element simulation. The ambient pressure of 20 kPa-1 atm could be detected by measuring the resonant frequency of big cells which was less affected by the changes of RH. Once the pressure was determined, the humidity performance would be analyzed through the resonant frequency shifts of small coated cells in a RH range of 30 %–90 %. The coated small cells exhibited good sensitivity at different pressures and decent repeatability under the same conditions. Hence the dual-frequency CMUT sensor can improve the humidity measurement accuracy by correcting the effect of pressure variation on its performance and is also an excellent candidate for simultaneous detection of pressure and RH.

CRediT authorship contribution statement

Xiaoli Zhang: Conceptualization, Methodology, Investigation, Writing - original draft. **Xingguo Zhang:** Methodology, Investigation. **Xiaochen Lai:** Software, Visualization. **Ridong Wang:** Formal analysis, Software. **Haixia Yu:** Supervision, Writing - review & editing. **Dachao Li:** Supervision, Writing - review & editing, Funding acquisition.

Declaration of Competing Interest

The authors declare that they have no known competing financial interests or personal relationships that could have appeared to influence the work reported in this paper.

Acknowledgements

This work was supported by the National Key R&D Program of China [No. 2018YFE0205000, No. 2017YFA0205103]; the National Natural Science Foundation of China [No. 81571766], the Natural Science Foundation of Tianjin [No. 17JCYBJC24400], and the 111 Project of China [No. B07014].

References

[1] H. Tang, Y. Li, H. Ye, F. Hu, C. Gao, L. Tao, T. Tu, G. Gou, X. Chen, X. Fan, T. Ren, G. Zhang, High-performance humidity sensor using Schottky-contacted SnS nanoflakes for noncontact healthcare monitoring, Nanotechnology 31 (5) (2020) 055501.
[2] X.-L. Gu, Z. Dong, Q. Yuan, W.-P. Zhang, Corrosion of stirrups under different relative humidity conditions in concrete exposed to chloride environment, J. Mater. Civ. Eng. 32 (1) (2020) 04019329.
[3] T. Ozden, A.J. Carr, B. Geerligs, R. Turan, B.G. Akinoglu, One-year performance evaluation of two newly developed back-contact solar modules in two different climates, Renew. Energy 145 (2020) 557–568.
[4] S.R.M. Coelho, E.G. Alves Filho, L.M.A. Silva, T.Z. Bischoff, P.R.V. Ribeiro, G.J. Zocolo, K.M. Canuto, P.Z. Bassinello, E.S. de Brito, NMR and LC-MS assessment of compound variability of common bean (Phaseolus vulgaris) stored under controlled atmosphere, Lwt-Food Sci. Technol. 117 (2020) 108673.
[5] B. Li, Q. Tian, H. Su, X. Wang, T. Wang, D. Zhang, High sensitivity portable capacitive humidity sensor based on In2O3 nanocubes-decorated GO nanosheets and its wearable application in respiration detection, Sens. Actuators B-Chem. 299 (2019) 126973.
[6] A. Hashim, Y. Al-Khafaji, A. Hadi, Synthesis and characterization of flexible resistive humidity sensors based on PVA/PEO/CuO nanocomposites, Trans. Electr. Electron. Mater. 20 (6) (2019) 530–536.
[7] K.-L. Chan, M.-H. Yang, H.-T. Chiu, C.-Y. Lee, Considerable humidity response of a well-aligned SOMS micro-wire flexible sensor by moisture-induced releasing of trapped electrons, Dalton Trans. 46 (33) (2017) 10859–10866.
[8] Y.-G. Han, Relative humidity sensors based on microfiber knot resonators-A review, Sensors (Basel, Switzerland) 19 (23) (2019) 5196.
[9] J. Xu, M. Bertke, H.S. Wasisto, E. Peiner, Piezoresistive microcantilevers for humidity sensing, J. Micromech. Microeng. 29 (5) (2019) 053003.
[10] Z. Zheng, Y. Yao, Y. Sun, J.T.W. Yeow, Development of a highly sensitive humidity

sensor based on the capacitive micromachined ultrasonic transducer, Sens. Actuators B Chem. 286 (2019) 39–45.
[11] C.-Y. Lee, G.-B. Lee, Humidity sensors: a review, Sens. Lett. 3 (1) (2005) 1–14.
[12] H. Farahani, R. Wagiran, M.N. Hamidon, Humidity sensors principle, mechanism, and fabrication technologies: a comprehensive review, Sensors 14 (2014) 7881–7939.
[13] S. Wang, G. Xie, Y. Su, L. Su, Q. Zhang, H. Du, H. Tai, Y. Jiang, Reduced graphene oxide-polyethylene oxide composite films for humidity sensing via quartz crystal microbalance, Sens. Actuators B-Chem. 255 (2018) 2203–2210.
[14] T. Mirea, E. Iborra, V. Yantchev, Microacoustic in-liquid sensors based on thin AlN films: a comparative study, IEEE International Ultrasonics Symposium Proceedings (2014) 659–662.
[15] X. Le, X. Wang, J. Pang, Y. Liu, B. Fang, Z. Xu, C. Gao, Y. Xu, J. Xie, A high performance humidity sensor based on surface acoustic wave and graphene oxide on AlN/Si layered structure, Sens. Actuators B Chem. 255 (2018) 2454–2461.
[16] D. Li, X. Zu, D. Ao, Q. Tang, Y. Fu, Y. Guo, K. Bilawal, M.B. Faheem, L. Li, S. Li, Y. Tang, High humidity enhanced surface acoustic wave (SAW) H2S sensors based on sol-gel CuO films, Sens. Actuators B-Chem. 294 (2019) 55–61.
[17] W. Xuan, M. Cole, J.W. Gardner, S. Thomas, F.-H. Villa-López, X. Wang, S. Dong, J. Luo, A film bulk acoustic resonator oscillator based humidity sensor with graphene oxide as the sensitive layer, J. Micromech. Microeng. 27 (2017) 055017.
[18] Y. Guan, X. Le, M. Hu, W. Liu, J. Xie, A noninvasive method for monitoring respiratory rate of rats based on a microcantilever resonant humidity sensor, J. Micromech. Microeng. 29 (12) (2019) 125001.
[19] Z. Zheng, Y. Yao, J.A. Liu, Y. Sun, J.T.W. Yeow, Highly sensitive CMUT-based humidity sensors built with nitride-to-oxide wafer bonding technology, Sens. Actuators B Chem. 294 (2019) 123–131.
[20] L. Zhao, Y. Zhao, Y. Xia, Z. Li, J. Li, J. Zhang, J. Wang, X. Zhou, Y. Li, Y. Zhao, Z. Jiang, A novel CMUT-based resonant biochemical sensor using electrospinning technology, IEEE Trans. Ind. Electron. 66 (9) (2019) 7356–7365.
[21] C. Seok, M.M. Mahmud, M. Kumar, O.J. Adelegan, F.Y. Yamaner, a.Ö. Oralkan, A low-power wireless multichannel gas sensing system based on a capacitive micromachined ultrasonic transducer (cmut) array, IEEE Internet Things J. 6 (1) (2019) 831–843.
[22] H.J. Lee, K.K. Park, M. Kupnik, N.A. Melosh, B.T. Khuri-Yakub, Mesoporous thin-film on highly-sensitive resonant chemical sensor for relative humidity and co2 detection, Anal. Chem. Lett. 84 (2012) 3063–3066.
[23] H.J. Lee, K.K. Park, Ö. Oralkan, M. Kupnik, B.T. Khuri-Yakub, A multichannel oscillator for a resonant chemical sensor system, IEEE Trans. Ind. Electron. 61 (10) (2014) 5632–5640.
[24] Q. Stedman, K.K. Park, B.T. Khuri-Yakub, CMUT chip with integrated temperature and pressure sensors, IEEE International Ultrasonics Symposium Proceedings (2016) 1–4.
[25] S.-W. Lee, B.I. Choi, S.-B. Woo, J.C. Kim, Y.-G. Kim, Calibration of a radiosonde humidity sensor at low temperature and low pressure, Metrologia 56 (5) (2019) 055008.
[26] M.-C. Ho, M. Kupnik, K.K. Park, K. Eckhoff, B.T. Khuri-Yakub, Wide pressure range operation of air-coupled CMUTs, 2012 Ieee International Ultrasonics Symposium (2012) 93–96.
[27] N. Apte, K.K. Park, B.T. Khuri-Yakub, Experimental evaluation of CMUTs with vented cavities under varying pressure, 2013 Ieee International Ultrasonics Symposium (2013) 1724–1727.
[28] Z. Li, L. Zhao, Z. Jiang, S. Akhbari, J. Ding, Y. Zhao, Y. Zhao, L. Lin, Capacitive micromachined ultrasonic transducer for ultra-low pressure measurement: theoretical study, AIP Adv. 5 (12) (2015) 127231.
[29] X. Zhang, L. Yu, Q. Guo, D. Li, H. Zhang, H. Yu, Resonance frequency analysis of a dual-frequency capacitive micromechanical ultrasonic transducer for detecting high and low pressures simultaneously with high sensitivity and linearity, J. Phys. D-Appl. Phys. 53 (3) (2020) 035401.
[30] D.-H. Kim, D. Son, J. Kim, Stretchable inorganic nanomembrane electronics for healthcare devices, in: T. George, A.K. Dutta, M.S. Islam (Eds.), Micro- and Nanotechnology Sensors, Systems, and Applications Vii, Vol. 9467 2015.
[31] Y. Javed, M. Mansoor, I.A. Shah, A review of principles of MEMS pressure sensing with its aerospace applications, Sens. Rev. 39 (5) (2019) 652–664.
[32] S. Fan, K. Jeong, V.P. Wallace, Z. Aman, Use of terahertz waves to monitor moisture content in high-pressure natural gas pipelines, Energy Fuels 33 (9) (2019) 8026–8031.
[33] Y. Sun, K. Kirimoto, H. Hattori, Y. Kitamura, E. Fan, K. Onishi, Electric field and oxygen concentration-dependent transport properties of nano-graphene oxide, AIP Adv. 9 (9) (2019) 9095010.
[34] A.S. Ergun, Y.L. Huang, X.F. Zhuang, O. Oralkan, G.G. Yaralioglu, B.T. Khuri-Yakub, Capacitive micromachined ultrasonic transducers: fabrication technology, IEEE Trans. Ultrason. Ferroelectr. Freq. Control 52 (12) (2005) 2242–2258.
[35] R. Maity, K. Gogoi, N.P. Maity, Micro-electro-mechanical-system based capacitive ultrasonic transducer as an efficient immersion sensor, Microsyst. Technol.-Micro Nanosyst.-Inf. Storage Proc. Syst. 25 (12) (2019) 4663–4670.
[36] G.G. Yaralioglu, A.S. Ergun, B. Bayram, E. Haeggstrom, B.T. Khuri-Yakub, Calculation and measurement of electromechanical coupling coefficient of capacitive micromachined ultrasonic transducers, IEEE Trans. Ultrason. Ferroelectr. Freq. Control 50 (4) (2003) 449–456.
[37] W. Zhang, H. Zhang, F. Du, J. Shi, S. Jin, Z. Zeng, Pull-in analysis of the flat circular CMUT cell featuring sealed cavity, Math. Probl. Eng. (2015) 150279.
[38] K.K. Park, H. Lee, M. Kupnik, O. Oralkan, J.-P. Ramseyer, H.P. Lang, M. Hegner, C. Gerber, B.T. Khuri-Yakub, Capacitive micromachined ultrasonic transducer (CMUT) as a chemical sensor for DMMP detection, Sens. Actuators B-Chem. 160 (1) (2011) 1120–1127.
[39] H.J. Lee, K.K. Park, M. Kupnik, B.T. Khuri-Yakub, Functionalization layers for CO2 sensing using capacitive micromachined ultrasonic transducers, Sens. Actuators B-Chem. 174 (2012) 87–93.
[40] Z. Li, L. Zhao, Z. Ye, H. Wang, Y. Zhao, Z. Jiang, Resonant frequency analysis on an electrostatically actuated microplate under uniform hydrostatic pressure, J. Phys. D-Appl. Phys. 46 (19) (2013) 195108.
[41] P. Zhang, G. Fitzpatrick, T. Harrison, W.A. Moussa, R.J. Zemp, Double-SOI wafer-bonded CMUTs with improved electrical safety and minimal roughness of dielectric and electrode surfaces, J. Microelectromech. Syst. 21 (3) (2012) 668–680.
[42] C. Steffens, A. Manzoli, F.L. Leite, O. Fatibello, P.S.P. Herrmann, Atomic force microscope microcantilevers used as sensors for monitoring humidity, Microelectron. Eng. 113 (2014) 80–85.

Xiaoli Zhang received the B.S. degree in Measurement and Control Technology and Instrument, North University of China, Taiyuan, China, in 2012. She is currently pursuing the Ph.D. degree in the college of precision instrument and opto-electronics engineering at Tianjin University, Tianjin, China. Her research interests focus on chemical sensing applications based on CMUT sensor.

Xingguo Zhang received the B.S. degree in Measurement and Control Technology and Instrument, Hefei University of Technology, Hefei, China, in 2016. And he is currently pursuing the Ph.D. degree in the college of precision instrument and opto-electronics engineering at Tianjin University, Tianjin, China. His research interests focus on biosensors.

Xiaochen Lai received his B.S. degree in Measuring and Controlling Technology and Instrument from Beijing Information Science & Technology University, Beijing, China, in 2014. And he is currently pursuing the Ph.D. degree in the college of precision instrument and opto-electronics engineering at Tianjin University, Tianjin, China. His research interest includes inkjet printing techniques and microfluidics.

Ridong Wang received his B.S. and M.S. degrees in School of Precision Instruments and Optoelectronics Engineering, Tianjin University, Tianjin, China, in 2011 and 2014, respectively. And he received the Ph.D. degree in Mechanical Engineering, Iowa State University, Iowa, US, in 2019. Currently, he is an associate professor in School of Precision Instruments and Optoelectronics Engineering, Tianjin University. His research interests include Raman-based study of micro/nanoscale structure and thermal transport, flexible biosensors.

Haixia Yu received her doctoral degree in 2011 from Tianjin University, Tianjin, China. Currently, she is an associate professor in the College of Precision Instruments and Optoelectronics Engineering, Tianjin University. Her research interests focus on biomedical microfluidics and biomedical micro-sensors.

Dachao Li received a B.S. degree in precision instruments from Tianjin University, Tianjin, China, in 1998 and M.S. and Ph.D. degrees in precision instruments and mechanics from Tianjin University, Tianjin, China, in 2001 and 2004, respectively. Li was previously a research associate at the Department of Electrical Engineering and Computer Science, Case Western Reserve University, Cleveland, Ohio, USA. Currently, he is a professor and Ph.D. supervisor in the College of Precision Instruments and Optoelectronics Engineering, Tianjin University. His research interests focus on micro-sensors and optofluidics.